Infrared Studies of Combined Resonance in *n*-Type InSb

B. D. McCombe
Naval Research Laboratory, Washington, D. C. 20390
(Received 2 December 1968)

The combined resonance absorption line involving a change in both Landau (L) and spin (S) quantum numbers ($\Delta L=1$; $\Delta S=-1$) has been studied in several samples of n-type InSb having carrier concentrations between 10^{14} and 10^{16} cm^{-3}. Experiments were performed at liquid-nitrogen and liquid-helium temperatures in magnetic fields between 10 and 100 kG. Measurements of the integrated absorption of this line as a function of magnetic field and carrier concentration are compared with calculations based on the nonparabolicity and inversion-asymmetry mechanisms. Results are in good agreement with the predictions of the nonparabolicity mechanism, indicating that this is the primary mechanism allowing such transitions in InSb. The observed combined resonance transition in conjunction with spin-up and spin-down cyclotron resonance measurements have yielded the g values of the $L=0$ and $L=1$ Landau levels over a wide range of magnetic fields. None of the inversion-asymmetry-allowed transitions were observed. From this negative result, an upper bound is placed on the inversion-asymmetry parameter δ_0.

I. INTRODUCTION

THE free-carrier energy levels of a semiconductor placed in a uniform external magnetic field, neglecting spin-orbit coupling, are described simply by two sets of Landau levels (labeled by the quantum number L), one for spin parallel ($S=+\frac{1}{2}$) and one for spin antiparallel ($S=-\frac{1}{2}$) to the applied magnetic field. These two "Landau ladders" are displaced one from the other by an energy $g\beta H$, where g is the free-electron g value, β is the Bohr magneton, and H is the applied magnetic field.

The orbital motion of such a system is not coupled in any way to the spin degrees of freedom. When this system is perturbed by electromagnetic radiation, only two distinct sets of electronic transitions are allowed. In the dipole approximation (which is valid for all cases of interest), the electric part of the radiation field excites transitions in which the Landau quantum number L changes by ±1, and the spin quantum number S remains unchanged (cyclotron resonance). Similarly, the allowed magnetic-dipole-induced transitions are those in which the spin quantum number changes by ±1, and the Landau quantum number remains unchanged (electron spin resonance). These transitions are depicted in the schematic energy level diagram of Fig. 1 for a parabolic band.

When spin-orbit interaction is taken into account, the system is considerably more complicated. The free carriers now have an effective magnetic moment containing, in addition to the usual spin magnetic moment, an orbital moment which is, in fact, dominant in many cases. The energy levels of this system are described in terms of an effective g value and a generalized spin quantum number in the direction of the applied magnetic field. (In the following, g is taken to mean the *effective* g value in the sense that $g\beta H$ gives the energy separation between a pair of levels in a magnetic field that arises from the spin magnetic moment and spin-orbit coupling.[1]) In addition, and of primary importance to this discussion, there is a coupling between the orbital and spin motion of the carriers which breaks the simple selection rules described above. Transitions can now involve a change in both spin and Landau quantum numbers and can be excited by either the electric or magnetic component of the radiation. Such transitions are termed "combined resonance," and some possibilities are shown in Fig. 1.

In practice, the electric dipole interaction energy is always much greater than the magnetic dipole interaction energy, and the latter may be neglected. Hence in the remainder of this paper, the term "combined resonance" shall always refer to electric-dipole-excited transitions.

The precise nature of the coupling between spin and orbital motions via the spin-orbit interaction depends on details of the band structure and may be quite complicated. In general, in materials having large spin-orbit interaction, the coupling is expected to be appreciable where there is a lack of inversion symmetry or a small fundamental energy gap. A small energy gap between interacting bands always results in a large degree of nonparabolicity (terms of order k^4 and higher in the dependence of the electron energy $\mathcal{E}$ on the wave number k). Hence combined resonance transitions which are allowed due to large spin-orbit interaction and small energy gap have been termed "nonparabolicity"-allowed combined resonance. This terminology is not precise, however, since a band may be nonparabolic and *not* allow combined resonance transitions (when the spin-orbit interaction goes to zero).

In a series of papers, Rashba and Sheka have considered in detail the combined resonance transitions in semiconductors lacking an inversion center.[2,3] The particular case of InSb was treated using Kane's energy-band model,[4] and the combined resonance transition matrix elements were evaluated in terms of the

[1] Y. Yafet, in *Solid State Physics*, edited by F. Seitz and D. Turnbull (Academic Press Inc., New York, 1963), Vol. 14, p. 1.

[2] E. I. Rashba, Fiz. Tverd. Tela **2**, 1224 (1960) [English transl.: Soviet Phys.—Solid State **2**, 1109 (1960)].

[3] E. I. Rashba and V. I. Sheka, Fiz. Tverd. Tela **3**, 1735 (1961); **3**, 1863 (1961) [English transls.: Soviet Phys.—Solid State **3**, 1257 (1961); **3**, 1357 (1961)].

[4] E. O. Kane, J. Phys. Chem. Solids **1**, 249 (1957).

band parameters of this model. The first mention of the nonparabolicity mechanism for combined resonance was made by Yafet[1] for InSb. The calculation of the electric dipole matrix elements was outlined and an estimate was made of their magnitudes at microwave frequencies, but detailed calculations were not presented. A detailed treatment of the nonparabolicity-allowed combined resonance for electric dipole radiation was given independently by Sheka[5] also for InSb. (Hasegawa and Sasada[6] have recently pointed out a correction term in the velocity matrix element for combined resonance transitions due to the "anomalous velocity" of Bloch electrons in an external magnetic field.) In addition, Bell and Rogers[7] have performed a computer calculation of the combined resonance matrix elements for InSb which includes both inversion-asymmetry and nonparabolicity effects.

Calculations of the combined resonance matrix elements for other materials include Boiko's work[8] for the L-point conduction bands of Ge and Wolff's[9] treatment of the matrix elements and selection rules for combined resonance transitions in the bismuth conduction band on the basis of the two-band model of Cohen and Blount.[10]

There have been few experimental studies of combined resonance to date. Bell[11] has reported the observation of the conduction-electron paramagnetic resonance transition induced by electric dipole radiation in InSb at microwave frequencies, and it also appears that Bemski's[12] paramagnetic resonance measurements in InSb may have been electric-dipole-induced, since a large plasma-shifted cyclotron resonance appears in his data. Bratashevskii *et al.*[13] have reported four absorption lines in InSb at liquid-oxygen temperatures excited by microwave electric dipole radiation with the electric vector parallel to the applied magnetic field. They attributed these lines to combined resonance absorptions; however, this interpretation is subject to question for a number of reasons. In particular, the lines they observe occur in the magnetic field region between 4000 and 7000 G, while at the frequency of observation the calculated positions of these lines lie between 150 and 500 G.[14] This discrepancy cannot be attributed to a plasma shifting of the resonance peaks as was suggested,[13] since plasma effects, if present, would shift the lines to *lower* fields, not higher fields.

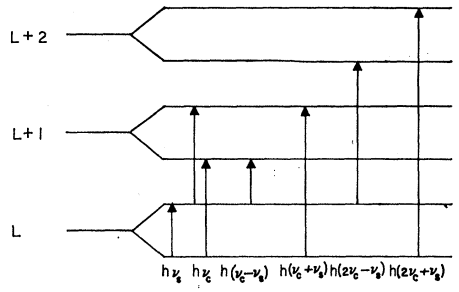

FIG. 1. Schematic energy-level diagram for a parabolic band in a magnetic field including the effects of spin. The cyclotron energy $h\nu_c$ and spin energy $h\nu_s$ are the same for all Landau levels L.

Absorption peaks have also been observed in the far-infrared transmission of bismuth in a magnetic field.[15] These peaks were attributed to combined resonance transitions. Very recently Hensel[16] has reported combined resonance transitions in the valence band of uniaxially stressed Ge. Aside from confirming the existence of combined resonance, none of these experiments provides direct comparison with theory.

Since the majority of existing calculations concern InSb and experimental data are scarce, this material seemed a natural choice for a detailed experimental study. The experiments reported in this paper are an extension of the original observation of the combined resonance transition with $\Delta L=1$ and $\Delta S=-1$ by the present authors.[17] In Sec. II, the theory of combined resonance is outlined for both the inversion-asymmetry and nonparabolicity mechanisms in InSb. Section III briefly discusses the experimental details. The experimental results are presented in Sec. IV, where the frequency and concentration dependence of the absorption are compared with theory. This represents the first systematic experimental study of combined resonance in a semiconductor and comparison of the results with theory. Results of the g-value measurements are also discussed in Sec. IV.

II. THEORY

The results of detailed combined resonance calculations of Rashba and Sheka[3,5] are presented in a general form with the absorption intensities given as ratios to the paramagnetic resonance intensity. As a result, comparison with infrared transmission experiments is somewhat inconvenient. Therefore a brief outline of the calculations for the two different mechanisms will be presented, concentrating primarily on the electric dipole matrix elements and integrated absorption for the experimentally observed transitions ($\Delta L=+1$, $\Delta S=-1$ and $\Delta L=0$, $\Delta S=-1$). The results are pre-

[5] V. I. Sheka, Fiz. Tverd. Tela **6**, 3099 (1964) [English transl.: Soviet Phys.—Solid State **6**, 2470 (1965)].
[6] H. Hasegawa and T. Sasada, Phys. Rev. **177**, 1392 (1969).
[7] R. L. Bell and K. T. Rogers, Phys. Rev. **152**, 746 (1966).
[8] I. I. Boiko, Fiz. Tverd. Tela **4**, 2128 (1962) [English transl.: Soviet Phys.—Solid State **4**, 1558 (1963)].
[9] P. Wolff, J. Phys. Chem. Solids **25**, 1057 (1964).
[10] M. Cohen and E. I. Blount, Phil. Mag. **5**, 115 (1960).
[11] R. L. Bell, Phys. Rev. Letters **9**, 52 (1962).
[12] G. Bemski, Phys. Rev. Letters **4**, 62 (1960).
[13] Yu. A. Bratashevskii, A. A. Galkin, and Yu. M. Ivanchenko, Fiz. Tverd. Tela **5**, 358 (1963) [English transl.: Soviet Phys.—Solid State **5**, 260 (1963)].
[14] E. I. Rashba, Usp. Fiz. Nauk **84**, 557 (1964) [English transl.: Soviet Phys.—Usp. **7**, 823 (1965)].
[15] J. C. Burgiel and L. C. Hebel, Phys. Rev. **140**, A925 (1965).
[16] J. C. Hensel, Phys. Rev. Letters **21**, 983 (1968).
[17] B. D. McCombe, S. G. Bishop, and R. Kaplan, Phys. Rev Letters **18**, 748 (1967).

sented in a form which is easily compared with the experimental measurements.

Indium antimonide possesses the zinc-blende crystal structure which lacks inversion symmetry. At the center of the Brillouin zone (Γ) the coefficients of the effective Hamiltonian are invariant under transformations by the tetrahedral group T_d. Ogg[18] has given the effective Hamiltonian in a magnetic field for the InSb conduction band to fourth order in k' at the Γ point. The effective Hamiltonian to this order is

$$\begin{aligned}\mathcal{H}_{C\rho C\rho'}=&\hbar^2\mathbf{k}'^2/2m^*+\tfrac{1}{2}g\beta\mathbf{H}\cdot\boldsymbol{\sigma}+\delta_0\boldsymbol{\sigma}\cdot\boldsymbol{\kappa}+\varepsilon_{xxxx0}\mathbf{k}'^4\\&+\alpha_0(\{k_x'^2,k_y'^2\}+\{k_x'^2,k_z'^2\}+\{k_y'^2,k_z'^2\})\\&+\beta_0\beta^2H^2+g_{xyyx}'\beta\boldsymbol{\sigma}\cdot\mathbf{H}\mathbf{k}'^2\\&+g_{xxyy}'\beta\{\boldsymbol{\sigma}\cdot\mathbf{k}',\mathbf{H}\cdot\mathbf{k}'\}+\gamma_0\beta\boldsymbol{\sigma}\cdot\boldsymbol{\tau},\quad(1)\end{aligned}$$

where

$$\mathbf{k}'=\mathbf{k}-e\mathbf{A}/\hbar c,$$

with the vector potential $\mathbf{A}=\frac{1}{2}\mathbf{H}\times\mathbf{r}$; ρ denotes the spin character of the band and may be $\uparrow$ or $\downarrow$; C denotes the conduction band; the components of $\boldsymbol{\sigma}$ are the Pauli spin matrices; $\kappa_x=k_y'k_x'k_y'-k_z'k_x'k_z'$ and cyclic permutations; $\tau_x=H_xk_x'^2$; m^*, g, δ_0, ε_{xxxx0}, α_0, β_0, g_{xyyx}', g_{xxyy}', and γ_0 are parameters which are related to interband momentum matrix elements and energy separations at $\mathbf{k}=0$ (m^* and g are the effective mass and g value, respectively, in the parabolic approximation, and the other terms represent higher-order corrections to the effective mass or g value); $\beta=|e|\hbar/2mc$ is the Bohr magneton; and the other symbols have their usual meanings.

It is easily seen by inspection that only the third and eighth terms in this Hamiltonian have nonzero off-diagonal matrix elements in the spin index and can thus be the origin of combined resonance transitions. The first of these terms is of order $\mathbf{k}'^3$ and is proportional to the parameter δ_0. This term is a result of inversion asymmetry in the zinc-blende structure and spin-orbit coupling. In the presence of inversion symmetry only terms of even order in $\mathbf{k}'$ are allowed in the Hamiltonian. The other term which is off-diagonal in the spin index is of fourth order in $\mathbf{k}'$ (the nonparabolicity term). Even though this is of higher order than the inversion-asymmetry term, it may give a larger contribution to the combined resonance matrix element. This may be seen from the following considerations: The major contribution to the parameter g_{xxyy}' comes from the doubly degenerate $\Gamma_{7,8}$ valence bands and the split off Γ_7 valence band which are separated by small energies from the conduction band; on the other hand, the major contribution to δ_0 (the inversion-asymmetry parameter) comes from the higher-lying conduction bands which are much farther removed in energy.

[18] N. R. Ogg, Proc. Phys. Soc. (London) 89, 431 (1966).

A. Velocity Matrix Elements and Selection Rules

1. Inversion Asymmetry

The velocity matrix elements involving a change in the spin state have been calculated by Rashba and Sheka[3] for the inversion-asymmetry mechanism when the corresponding term in the Hamiltonian of Eq. (1) may be treated as a perturbation on the parabolic Hamiltonian. The general result of this calculation for zinc-blende semiconductors is

$$\langle L;\downarrow|v_\alpha|J;\uparrow\rangle=\frac{\sqrt{2}\delta_0}{\hbar}k_H^2\frac{L-J-\eta}{L-J+q_\alpha-\eta}\times\sum_{\beta\gamma}B_{(\alpha\beta\gamma)}\langle L|a_\beta a_\gamma|J\rangle,\quad(2)$$

where J and L are the Landau quantum numbers of the initial and final states, respectively; $\alpha=1, 2, 3$ is the polarization index corresponding to left-circular, right-circular, and longitudinal ($\mathbf{E}\|\mathbf{H}$) polarization, respectively; $k_H=(eH/c\hbar)^{1/2}$; η is the ratio of the spin splitting to the cyclotron spacing in the parabolic approximation; $a_1=(1/\sqrt{2}k_H)(k_x'-ik_y')$, $a_2=(1/\sqrt{2}k_H)\times(k_x'+ik_y')$, and $a_3=k_z/k_H=\xi$ ($a_{1,2}$ are lowering and raising operators, respectively, for Landau levels); q_α is the change in Landau quantum number under the action of the operator a_α, i.e., $q_\alpha=-1$, 1, 0 as $a=1$, 2, 3; and the $B_{(\alpha\beta\gamma)}$ are trigonometric functions of the angle between the crystal axes and $\mathbf{H}$ which describe the anisotropy of the velocity matrix elements. Since the velocity matrix elements of Eq. (2) are proportional to the product of two of the a_α operators taken between Landau states, spin-flip transitions are allowed in which the Landau quantum number changes by 0, 1, or 2. Such transitions are shown schematically in Fig. 1. In addition, each of these transitions is allowed for $\mathbf{E}\|\mathbf{H}$ or $\mathbf{E}\perp\mathbf{H}$, but the angular function is different, in general, for the different transitions and polarizations.

2. Nonparabolicity

The velocity matrix elements which correspond to the eighth term in the effective Hamiltonian of Eq. (1) have been calculated by Sheka[5] using the Hamiltonian of Bowers and Yafet,[19] which accurately accounts for the interaction of the conduction band with the nearest valence bands. The resulting velocity matrix elements are given by

$$\langle L;\downarrow|v_\alpha|J;\uparrow\rangle=\tfrac{2}{3}\pi\sqrt{2}|P|^2k_H\nu_{CR}[1/E_g^2-1/(E_g+\Delta)^2]\times[\xi\delta_{\alpha2}\delta_{JL}-\sqrt{(J+1)}\delta_{\alpha3}\delta_{L,J+1}],\quad(3)$$

where E_g is the fundamental energy gap, Δ is the spin-orbit energy parameter, P is the conduction-valence band momentum matrix element; $\nu_{CR}=\nu_s$ for $\Delta J=0$, $\nu_{CR}=\nu_{c,s}$ ($=\nu_c+\nu_s$ in the parabolic approximation) for $\Delta J=1$; and the rest of the symbols have been defined

[19] R. Bowers and Y. Yafet, Phys. Rev. 115, 1165 (1959).

previously. In contrast to the inversion-asymmetry matrix elements, the matrix elements of Eq. (3) are isotropic, except for the weak dependence of the transition frequency (ν_{CR}) on orientation. In addition there are only two allowed combined resonance transitions in this case; one for right-circular polarization (at the spin resonance frequency), and one for $\mathbf{E}\|\mathbf{H}$ (at a frequency equal to the sum of the cyclotron and spin resonance frequencies).

B. Integrated Absorption

The absorptive part of the response of a system to electromagnetic radiation is described by the imaginary part of the dielectric function, $\epsilon''(\omega)$. Neglecting broadening, this may be written in terms of velocity matrix elements by

$$\epsilon_a''(\omega)=\frac{4\pi^2e^2}{V\omega^2}\sum_{nm}|\mathbf{a}\cdot\mathbf{v}_{nm}|^2\times[f(n)-f(m)]\delta[\hbar(\omega-\omega_{nm})], \quad (4)$$

where n and m denote the initial and final states of the transition, respectively; $\hbar\omega_{nm}$ is the energy difference between initial and final states, ω is the angular frequency of the electromagnetic radiation, $\mathbf{a}$ is a unit polarization vector of the radiation, $f(k)$ is the probability of occupation of the kth state, V is the volume of the material, and e is the electronic charge in electrostatic units. Converting the sum to an integral and assuming a parabolic energy-momentum relation for simplicity in calculation (using primarily the notation of Ref. 3),

$$\epsilon_\alpha''(\omega)=\frac{e^2k_H{}^3}{\omega^2}\sum_J\int d\xi|\langle J+\Delta J;-S|v_\alpha|J;S\rangle|^2\times[f(J,S,\xi)-f(J+\Delta J,-S,\xi)]\times\delta[\hbar(\omega-\omega_{J,S;J+\Delta J,-S})], \quad (5)$$

where

$$f(J,S,\xi)=1/(e^{\lambda(J+1/2+S\eta+\xi^2/2-\zeta)}+1);$$

$\lambda=\hbar\omega_c/k_BT$; $\zeta=\mu/\hbar\omega_c$= the chemical potential in units of $\hbar\omega_c$; and J is the Landau quantum number of the initial state. The integrated absorption (integrated over magnetic field) is obtained as

$$\alpha\Delta H=\int\frac{\omega}{cn}\epsilon''(\omega,H)dH, \quad (6)$$

where n is the refractive index. Here $\alpha\Delta H$ is the fractional power lost per unit length by the electromagnetic wave of frequency ω at all magnetic fields.

The summation and integration indicated in Eq. (5) are easily performed for two cases: (a) nondegenerate electron gas, and (b) degenerate electron gas with low concentration, i.e., all electrons are in the lowest Landau level and lowest spin state. These cases will be treated in turn for the nonparabolicity and inversion-asymmetry mechanisms and the results compared.

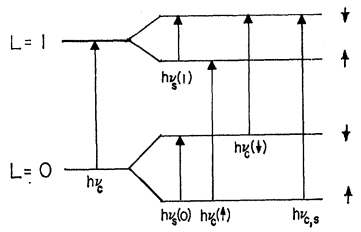

FIG. 2. Schematic energy-level diagram for the nonparabolic conduction band of InSb showing the lowest two Landau levels including spin. The energies of interest are labeled.

1. Nondegenerate

For nondegenerate statistics the Fermi function becomes

$$f(J,S,\xi)=e^{\lambda(\zeta+S|\eta|-J-1/2-\xi^2/2)},$$

where the fact that the g value, and hence η, is negative for InSb has been used. The condition requiring conservation of total number of carriers is written

$$N=\frac{k_H{}^3}{4\pi^2}\sum_J\int d\xi(e^{\lambda(\zeta+|\eta|/2-J-1/2-\xi^2/2)}+e^{\lambda(\xi-|\eta|/2-J-1/2-\xi^2/2)}),$$

yielding for the chemical potential

$$e^{\lambda\zeta}=\frac{2\pi(2\pi\lambda)^{1/2}N}{k_H{}^3}\frac{\sinh\frac{1}{2}\lambda}{\cosh\frac{1}{2}\lambda|\eta|}. \quad (7)$$

(a) *Nonparabolicity.* From Eq. (3) for $\mathbf{E}\|\mathbf{H}$ there is an allowed velocity matrix element for transitions involving a change in both Landau and spin quantum numbers ($\Delta L=1$; $\Delta S=-1$) given by

$$\langle L+1;\downarrow|v_3|L;\uparrow\rangle_{NP}=-\tfrac{2}{3}\sqrt{2}|P|^2[1/E_g{}^2-1/(E_g+\Delta)^2]\times\sqrt{(L+1)k_H}\nu_{c,s}, \quad (8)$$

where $h\nu_{c,s}$ is the transition energy corresponding to $\Delta L=1$, $\Delta S=-1$ as shown in Fig. 2. Substituting in Eq. (5), performing the indicated summation and integration, and using Eq. (7) for the chemical potential, the following result is obtained:

$$\epsilon_3''(\omega)_{NP}=(4\pi^2|P|^4e^2/9)[1/E_g{}^2-1/(E_g+\Delta)^2]^2Nk_H{}^2\times[1+\coth\tfrac{1}{2}\lambda/\coth\tfrac{1}{2}\lambda|\eta|]\delta[\hbar(\omega-\omega_{c,s})]. \quad (9)$$

From Eq. (6) the integrated absorption is given by

$$(\alpha_3\Delta H)_{NP}=\frac{4\pi|P|^4e^3}{9c^3\hbar^2n}\left[\frac{1}{E_g{}^2}-\frac{1}{(E_g+\Delta)^2}\right]^2\times NH^2\left[1+\frac{\coth\frac{1}{2}\lambda}{\coth\frac{1}{2}\lambda|\eta|}\right]. \quad (10)$$

Similarly, for right-circular polarization there is an

allowed velocity matrix element having transition energy $h\nu_s(\Delta L=0;\ \Delta S=-1)$ given by

$$\langle L;\downarrow|v_2|L;\uparrow\rangle_{\mathrm{NP}}=\tfrac{2}{3}\sqrt{2}\,|P|^2 \times[1/E_g^2-1/(E_g+\Delta)^2]k_H\nu_s\xi. \quad (11)$$

The imaginary part of the dielectric constant for this transition is

$$\epsilon_2''(\omega)_{\mathrm{NP}}=\frac{4\pi^2|P|^4e^2}{9}\left[\frac{1}{E_g^2}-\frac{1}{(E_g+\Delta)^2}\right]^2 \times Nk_H^2\frac{\tanh\tfrac{1}{2}\lambda|\eta|}{\tfrac{1}{2}\lambda}\delta[\hbar(\omega-\omega_s)], \quad (12)$$

and the integrated absorption is

$$(\alpha_2\Delta H)_{\mathrm{NP}}=\frac{8\pi^2|P|^4e^3}{9c^2\hbar^2n}\left[\frac{1}{E_g^2}-\frac{1}{(E_g+\Delta)^2}\right]^2\frac{NH^2}{\lambda} \times\tanh\tfrac{1}{2}\lambda|\eta|. \quad (13)$$

In the limiting case of large magnetic fields or low temperature (encountered in the experiments to be described), i.e., $\lambda\gg1$,

$$(\alpha_3\Delta H)_{\mathrm{NP}}\approx\frac{8\pi^2|P|^4e^3}{9c^2\hbar^2n}\left[\frac{1}{E_g^2}-\frac{1}{(E_g+\Delta)^2}\right]^2NH^2 \quad (14)$$

and

$$(\alpha_2\Delta H)_{\mathrm{NP}}\approx\frac{8\pi^2|P|^4e^2}{9ch^3n} \times m_c\left[\frac{1}{E_g^2}-\frac{1}{(E_g+\Delta)^2}\right]^2k_BTNH. \quad (15)$$

(*b*) *Inversion asymmetry.* In order to provide easy comparison with the nonparabolicity results, only those matrix elements from Eq. (2) having the same polarization and transition energy as the allowed nonparabolicity matrix elements will be considered in detail.

For $\mathbf{E}\|\mathbf{H}$ at transition energy $h\nu_{c,s}$ the inversion-asymmetry matrix element is

$$\langle L+1;\downarrow|v_3|L;\uparrow\rangle=(2\sqrt{2}\delta_0/\hbar)k_H^2B_{(323)}\sqrt{(L+1)}\xi. \quad (16)$$

The corresponding imaginary part of the dielectric function and integrated absorption are given by

$$\epsilon_3''(\omega)_{\mathrm{IA}}=\frac{16\pi^2e^2\delta_0^2|B_{(323)}|^2}{\hbar^2\omega^2\lambda} \times\frac{Nk_H^4\sinh\tfrac{1}{2}(1+|\eta|)\lambda}{\sin\tfrac{1}{2}\lambda\cosh\tfrac{1}{2}\lambda|\eta|}\delta[\hbar(\omega-\omega_{c,s})] \quad (17)$$

and

$$(\alpha_3\Delta H)_{\mathrm{IA}}=\frac{16\pi^2e^2\delta_0^2|B_{(323)}|^2m_{c,s}^2}{ch^5n}\frac{NH}{\lambda} \times\frac{\sinh\tfrac{1}{2}(1+|\eta|)\lambda}{\sinh\tfrac{1}{2}\lambda\cosh\tfrac{1}{2}\lambda|\eta|}, \quad (18)$$

respectively.

For right-circular polarization there is a transition of energy $h\nu_s$ with matrix element given by

$$\langle L;\downarrow|v_2|L;\uparrow\rangle=(\sqrt{2}\delta_0k_H^2/4\hbar)[(2L+1)-2\xi^2]B_{(221)}. \quad (19)$$

Using this matrix element, the imaginary part of the dielectric function is calculated to be

$$\epsilon_2''(\omega)_{\mathrm{IA}}=\frac{8\pi^2e^2\delta_0^2|B_{(221)}|^2}{9\hbar^2\omega^2}k_H^4N\tanh\tfrac{1}{2}\lambda|\eta| \times\left[\frac{3}{4\lambda^2}-\frac{1}{4\lambda}(2+\coth\tfrac{1}{2}\lambda)+\tfrac{1}{4}\coth\tfrac{1}{2}\lambda+\tfrac{1}{8}\coth^2\tfrac{1}{2}\lambda+\tfrac{3}{16}\right] \times\delta[\hbar(\omega-\omega_s)], \quad (20)$$

and the integrated absorption is given by

$$(\alpha_2\Delta H)_{\mathrm{IA}}=\frac{8\pi^2e^2\delta_0^2m_c^2|B_{(221)}|^2}{\hbar^5cn}NH\tanh\tfrac{1}{2}\lambda|\eta| \times\left[\frac{3}{4\lambda^2}-\frac{1}{4\lambda}(2+\coth\tfrac{1}{2}\lambda)+\tfrac{1}{4}\coth\tfrac{1}{2}\lambda +\tfrac{1}{8}\coth^2\tfrac{1}{2}\lambda+\tfrac{3}{16}\right]. \quad (21)$$

In addition to transitions having the polarizations discussed above there are transitions for left- and right-circular polarization at energy $h\nu_{c,s}$ and transitions for left-circular polarization and $\mathbf{E}\|\mathbf{H}$ at energy $h\nu_s$. The dependence of the intensity on temperature, magnetic field, etc., is the same for all polarizations at a given transition energy, only the angular functions being different in each case. For $\alpha=1,2$ and energy $h\nu_{c,s}$, the corresponding intensities at the maximum of the angular functions are 3.38 and 0.19, respectively, times the intensity at the maximum of the angular function for Eq. (18). Similarly, at energy $h\nu_s$ the maximum intensity for $\alpha=1$ is 2.94 times and for $\alpha=3$, 13.2 times the maximum intensity for $\alpha=2$ [Eq. (21)].

For large magnetic fields (or low temperatures) $\lambda\gg1$, and Eqs. (18) and (21) may be written approximately

$$(\alpha_3\Delta H)_{\mathrm{IA}}\approx[128\pi^2em_cm_{c,s}^2/3n\hbar^6]\delta_0^2Nk_BT \quad (22)$$

and

$$(\alpha_2\Delta H)_{\mathrm{IA}}\approx[3\pi^2e^2m_c^2/2h^5cn]\delta_0^2NH, \quad (23)$$

for $\mathbf{H}\|\langle111\rangle$ axis ($|B_{(323)}|^2=\frac{4}{3}$; $|B_{(221)}|^2=\frac{1}{3}$).

These results are to be compared with Eqs. (14) and (15) for the nonparabolicity mechanism. In this limit the integrated intensity for $\mathbf{E}\|\mathbf{H}$ at energy $h\nu_{c,s}$ is proportional to H^2 for the nonparabolicity mechanism and is *independent* of H for the inversion-asymmetry mechanism. For right-circular polarization at the spin resonance energy, the integrated intensity is proportional to H for both mechanisms.

The complete results as expressed in Eqs. (10) and (13), and Eqs. (18) and (21) are shown graphically in

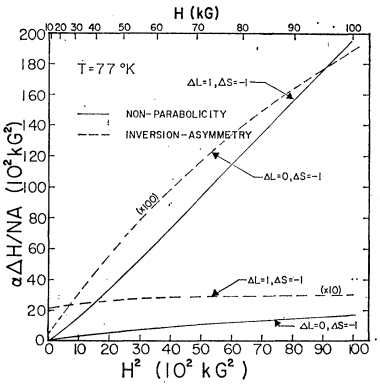

FIG. 3. Plots of calculated integrated absorption versus H^2 for the combined resonance transitions of energy $h\nu_{c,s}$ ($\Delta L=1$; $\Delta S=-1$) and $h\nu_s(0)$ ($\Delta L=0$; $\Delta S=-1$) in the nondegenerate limit. The constant A is defined in the text.

Fig. 3. Here the integrated intensity divided by

$$A=\frac{4\pi^2|P|^4e^3}{9c^2\hbar^2n}\left[\frac{1}{E_g^2}-\frac{1}{(E_g+\Delta)^2}\right]^2$$

is plotted versus H^2. At high fields, the strongest transition by far is for $\mathbf{E}\|\mathbf{H}$ at $h\nu_{c,s}$ allowed by nonparabolicity. The intensity of the corresponding transition for the inversion-asymmetry mechanism is weaker by greater than a factor of 50 at 90 kG for the parameters used in this calculation. The relative intensities of the other transitions are obvious from the graph. In general, for magnetic fields greater than 10 or 20 kG, transitions allowed by the nonparabolicity mechanism are much stronger than the corresponding transitions allowed by the inversion-asymmetry mechanism.

2. *Degenerate: Low Concentration*

For a degenerate electron gas with sufficiently low concentration and in a high magnetic field, only the lowest Landau level with spin up is populated. In this simplified situation the relation between the number of carriers and the chemical potential is given by

$$[\zeta+\tfrac{1}{2}|\eta|-\tfrac{1}{2}]^{1/2}=\sqrt{2}\pi^2N/k_H^3. \tag{24}$$

The necessary condition that only the lowest level be populated is

$$\pi^2N/k_H^3<1/\sqrt{6}, \tag{25}$$

since $|\eta|\simeq\frac{1}{3}$ for InSb. This condition is satisfied for magnetic fields greater than about 4 kG for a carrier concentration of 6×10^{14} cm^{-3} and for magnetic fields greater than about 20 kG for a concentration of 6×10^{15} cm^{-3}.

(*a*) *Nonparabolicity.* Equation (8) gives the velocity matrix element with transition energy $h\nu_{c,s}(\Delta L=1;\ \Delta S=1)$ for $\mathbf{E}\|\mathbf{H}$. Substituting this in Eq. (5) and using Eq. (24), we obtain for the imaginary part of the dielectric constant

$$\epsilon_3''(\omega)_{\mathrm{NP}}=\frac{8\pi^2|P|^4e^2}{9}\left[\frac{1}{E_g^2}-\frac{1}{(E_g+\Delta)^2}\right]^2\times k_H^2N\delta[\hbar(\omega-\omega_{c,s})]. \tag{26}$$

The corresponding integrated absorption is given by

$$(\alpha_3\Delta H)_{\mathrm{NP}}=\frac{8\pi^2|P|^4e^3}{9\hbar^2c^2n}\left[\frac{1}{E_g^2}-\frac{1}{(E_g+\Delta)^2}\right]^2NH^2. \tag{27}$$

For right-circular polarization, the allowed velocity matrix element has transition energy $h\nu_s(\Delta L=0;\ \Delta S=-1)$ and is given by Eq. (11). The imaginary part of the dielectric constant for this transition is

$$\epsilon_2''(\omega)_{\mathrm{NP}}=\frac{32\pi^6|P|^4e^2}{27}\times\left[\frac{1}{E_g^2}-\frac{1}{(E_g+\Delta)^2}\right]^2\frac{N^3}{k_H^4}\delta[\hbar(\omega-\omega_s)]. \tag{28}$$

From Eq. (6) the integrated absorption is obtained as

$$(\alpha_2\Delta H)_{\mathrm{NP}}=\frac{32\pi^6|P|^4ch}{27n}\left[\frac{1}{E_g^2}-\frac{1}{(E_g+\Delta)^2}\right]\frac{N^3}{H}. \tag{29}$$

Comparison of these results with the results obtained in the previous section for the nondegenerate case shows that for transition energy $h\nu_{c,s}$, the result expressed by Eq. (27) is identical to the result in the nondegenerate case in the limit $\lambda\gg1$, Eq. (14). This is to be expected since the velocity matrix element for this transition does not depend on k_z, and the different statistics yield the same result under these approximations due to the normalization condition. On the other hand, the velocity matrix element for the transition at $h\nu_s$ depends on k_z, and the degenerate result has a drastically different dependence on carrier concentration and magnetic field than the corresponding result for the nondegenerate case, Eq. (15). In fact, in this case the transition intensity *decreases* as the magnetic field is increased.

Inserting numbers in Eqs. (15) and (28), we find for the ratio $(\alpha_2\Delta H)_{\mathrm{nondeg}}/(\alpha_2\Delta H)_{\mathrm{deg}}$ a value of approximately 1.5×10^3 for $T=77$°K, $H=50$ kG, $\lambda\gg1$, and $N=6\times10^{14}$ cm^{-3}. Hence lowering the temperature sufficiently to make the material degenerate causes a drastic reduction in intensity.

(*b*) *Inversion asymmetry.* The imaginary part of the dielectric constant for a transition of energy $h\nu_{c,s}(\Delta L=1;\ \Delta S=-1)$ with $\mathbf{E}\|\mathbf{H}$ is given by

$$\epsilon_3''(\omega)_{\mathrm{IA}}=\frac{128\pi^6e^2\delta_0^2m_c^2|B_{(323)}|^2N^3}{3\hbar^4k_H^6}\delta[\hbar(\omega-\omega_{c,s})]. \tag{30}$$

TABLE I. Calculated ratios of the nonparabolicity-allowed integrated absorption to inversion-asymmetry-allowed integrated absorption in the degenerate low-concentration limit for two different values of carrier concentration and magnetic field.

Carrier concentration	Transition energy	H(kG)	Ratio $=(\alpha\Delta H)_{NP}/(\alpha\Delta H)_{IA}$
$N=6\times10^{14}$ cm^{-3}	$h\nu_{c,s}$	50	1.45×10^{4}
	$h\nu_{s}$	50	4.4×10^{-2}
	$h\nu_{c,s}$	90	1.52×10^{5}
	$h\nu_{s}$	90	1.38×10^{-2}
$N=6\times10^{15}$ cm^{-3}	$h\nu_{c,s}$	50	1.45×10^{2}
	$h\nu_{s}$	50	4.4
	$h\nu_{c,s}$	90	1.62×10^{3}
	$h\nu_{s}$	90	1.38

The integrated absorption for this transition is

$$(\alpha_3\Delta H)_{IA}=\frac{128\pi^6\delta_0^2c^2m_c^2|B_{(323)}|^2}{3\hbar^2en}\frac{N^3}{H^2}. \quad (31)$$

Similarly for right-circular polarization the imaginary part of the dielectric function at transition energy $h\nu_s(\Delta L=0;\ \Delta S=-1)$ is given by

$$\epsilon_2''(\omega)_{IA}=\frac{8\pi^2e^2\delta_0^2m_c^2|B_{(212)}|^2N}{\hbar^4}\times\left[\frac{4\pi^8N^4}{k_H^{12}}-\frac{\pi^4N^2}{3k_H^6}+\frac{1}{16}\right]\delta[\hbar(\omega-\omega_s)], \quad (32)$$

and the corresponding integrated absorption by

$$(\alpha_2\Delta H)_{IA}=\frac{8\pi^2e^2\delta_0^2m_c^2|B_{(212)}|^2}{2\hbar^5cn}\times\left\{\frac{4\pi^8c^6\hbar^6N^5}{e^6H^5}-\frac{\pi^4c^3\hbar^3N^3}{3e^3H^2}+\frac{HN}{16}\right\}. \quad (33)$$

For reasonable values of magnetic field and concentration, the first and second terms in the curly brackets are negligible compared to the third term and the equation simplifies to

$$(\alpha_2\Delta H)_{IA}=\frac{\pi^2e^2\delta_0^2m_c^2|B_{(212)}|^2}{2\hbar^5cn}NH. \quad (34)$$

Since these inversion-asymmetry-induced transitions were not observed at either liquid-nitrogen or liquid-helium temperatures, their relative intensities will not be explicitly calculated. However, for additional comparison, the ratios of the nonparabolicity and the inversion-asymmetry-integrated absorptions obtained from the preceding equations are tabulated for several values of magnetic field and carrier concentration in Table I. It is obvious from the Table that for the transition at energy $h\nu_{c,s}$ the nonparabolicity mechanism dominates. On the other hand, the inversion-asymmetry mechanism is dominant for the transition at the spin resonance energy $h\nu_s$ at low concentrations with a *reversal* in relative intensity taking place at higher concentrations.

TABLE II. Characteristics of the n-type InSb samples used in the studies of integrated absorption.

Sample	N(cm^{-3}) 77°K	μ(cm^2/V sec) 77°K	Thickness (cm)	Degeneracy parameter 77°K
1	1.3×10^{14}	8.0×10^{5}	0.483	0.024
2	6.0×10^{14}	3.3×10^{5}	0.219	0.11
3	6.0×10^{15}	1.3×10^{5}	0.0813	1.1
4	1.5×10^{16}	5.1×10^{4}	0.0203	2.8

III. EXPERIMENTAL DETAILS

A. Samples

The n-type InSb samples used in these experiments were selenium-doped single crystals grown in this laboratory by Swiggard. The sample characteristics are presented in Table II. Carrier concentrations and mobilities were measured at liquid-N_2 temperature on Hall bars cut from material adjacent to the optical samples. These determinations are estimated to be accurate to about 10%. The samples used for the study of anisotropy were oriented by standard Laue x-ray techniques and cut on a spark cutter such that the sample faces were parallel to a {110} crystal plane. After polishing and mounting on the cold finger, the samples were again x rayed and found to be within 2° of the specified orientation.

B. Experimental Equipment

The high magnetic field (50–100 kG) infrared measurements were made in the NRL $2\frac{1}{2}$ in. Bitter magnet. Standard optical techniques were used, including selective crystal chopping, reststrahlen reflection plates, and a Perkin-Elmer grating monochrometer to obtain spectrally pure radiation in the wavelength range 16–35 μ.

The optical components and arrangement of the light beam were similar to those described by Palik *et al.*[20] Most of the measurements were made using a thermocouple detector and standard Perkin-Elmer electronics; however, several experimental runs were made with liquid-helium cooled copper-doped and zinc-doped germanium detectors in conjunction with a PAR HR-8 lock-in amplifier and a Mosley 7001A X-Y recorder. Polarized light with electric field vector **E** parallel or perpendicular to the applied magnetic field **H** was obtained with Perkin-Elmer wire-grid polarizers.

Samples were attached in the Voigt configuration to a copper cold finger fastened to the inner chamber of a tailed Dewar which was equipped with room-tempera-

[20] E. D. Palik, G. S. Picus, S. Teitler, and R. F. Wallis, Phys. Rev. 122, 475 (1961).

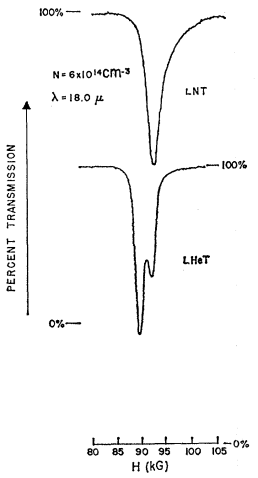

FIG. 4. Combined resonance transmission data for the transition of energy $h\nu_{c,s}$ ($\Delta L=1$; $\Delta S=-1$) in InSb. Top trace (left-hand scale) liquid-nitrogen temperature. Bottom trace (right-hand scale) liquid-helium temperature. The carrier concentration and wavelength are indicated in the figure.

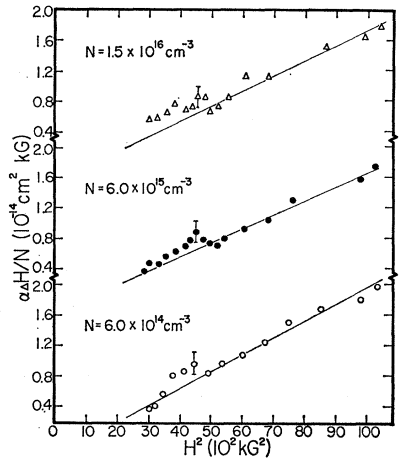

FIG. 5. Plots of integrated absorption versus H^2 for three samples of different carrier concentration. Data were obtained at liquid-nitrogen temperature. Approximate error bars are shown at one value of magnetic field. The straight lines are drawn through the data for reference purposes only, and are not the result of any calculation.

ture CsBr optical windows. Experiments were performed with liquid helium or liquid nitrogen in the inner chamber of the Dewar, and temperatures above the equilibrium boiling point of these two liquids could be obtained by means of a manganin wire heater wound on the cold finger. The temperature at the end of the cold finger was monitored with a calibrated germanium-resistance thermometer or a nominal 100 Ω, 1/10 W Allen-Bradley carbon resistor.

The lower-field measurements were made using a Fourier transform interferometric spectrometer and two superconducting magnet systems. The light pipes, sample holders, and detectors used with the interferometer have been described in detail by Kaplan.[21] Zinc-, beryllium-, and gallium-doped germanium photoconductive detectors were used at liquid-helium temperature to span the wavelength range 20–120 μ. One of the superconducting magnets provided magnetic fields up to about 34 kG in a 1-in. bore. The other system was capable of approximately 55 kG in a $1\frac{1}{4}$-in. bore. Both magnets were used in the persistent mode. All data were taken at 1-cm^{-1} resolution. Polarized light was obtained using small pieces of wire-grid polarizers fabricated by Hass[22] placed in the light beam immediately before the samples.

IV. EXPERIMENTAL RESULTS

Experiments were performed at both liquid-nitrogen and liquid-helium temperatures; however, most of the data to be discussed in this section were obtained at liquid-nitrogen temperature to avoid complicating effects of the "impurity-shifted" combined resonance line on the intensity measurements. At liquid-nitrogen temperature only the free-carrier line is important and a clear interpretation is possible.

These experiments are primarily concerned with the transition having energy $h\nu_{c,s}$ (Fig. 2) which was easily observable in samples having a wide range of concentrations. In addition a very weak transition was observed in one sample which is apparently the pure spin-flip transition $h\nu_s(0)$. Although numerous attempts were made, none of the transitions predicted by the inversion-asymmetry mechanism was observed. These results will be discussed with reference to the theoretical predictions of Sec. II.

Typical data for the transition at $h\nu_{c,s}$ are shown in Fig. 4 for $\mathbf{E}\|\mathbf{H}$ at both liquid-nitrogen and liquid-helium temperatures. As can be seen, a lower-field (higher-frequency) line appears in the liquid-helium temperature data; this is the localized electron transition. The field position of the free-carrier transition remained unchanged between liquid-nitrogen and liquid-helium temperature to within experimental error ($\sim 1\%$). Summers *et al.*[23] have observed a similar small variation ($<1\%$) in cyclotron resonance energy between liquid-nitrogen and liquid-helium temperatures. They explain this result as being due to the fact that the lattice constant is virtually the same at liquid-nitrogen and liquid-helium temperatures because the linear expansion coefficient for InSb changes sign at 57.5°K. The experiments are then in agreement with theory if only the dilational change in the energy gap is involved.

A. Intensity Measurements

For the transition at $h\nu_{c,s}$ with $\mathbf{E}\|\mathbf{H}$, a plot of the product of the peak absorption constant α and the full

[21] R. Kaplan, Appl. Opt. **6**, 685 (1967).
[22] M. Hass and M. O'Hara, Appl. Opt. **4**, 1027 (1965).
[23] C. J. Summers, R. B. Dennis, B. S. Wherrett, P. G. Harper, and S. D. Smith, Phys. Rev. **170**, 755 (1968).

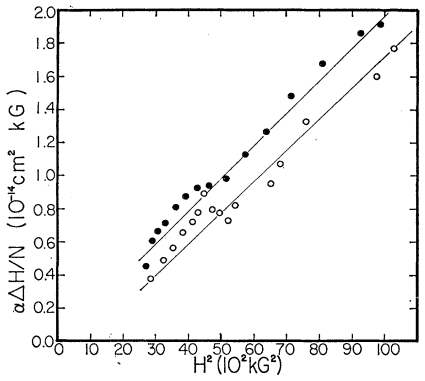

FIG. 6. Integrated absorption versus H^2 for a sample having $N=6\times10^{15}$ cm^{-3} at liquid-nitrogen temperature (open circles) and liquid-helium temperature (solid circles). The straight lines are included for reference.

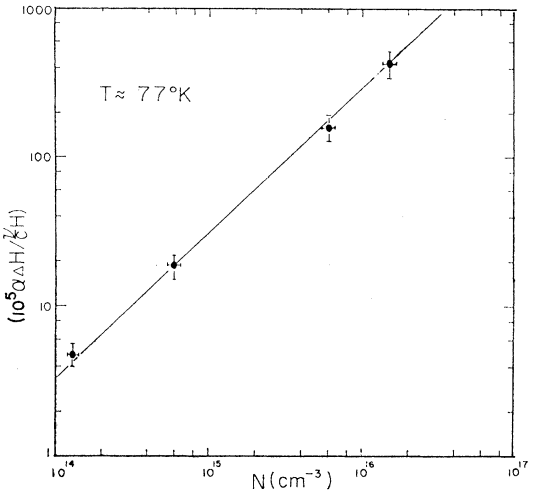

FIG. 7. A plot of the dimensionless parameter $\alpha\Delta H(\nu_{c,s}/c)H$ (proportional to integrated absorption) versus carrier concentration. The straight-line fit through the data has unity slope.

width at half-maximum (ΔH) divided by the carrier concentration N versus H^2 for three different samples at liquid-nitrogen temperature is shown in Fig. 5. The product $\alpha\Delta H$ as defined is considered to be a reasonable measure of the integrated absorption as calculated in Sec. II. The straight lines in the figure are drawn for reference purposes only and are not the result of any calculation. It is clear from these plots that except for the anomaly between 60 and 65 kG the experimental points fall on a reasonably good straight line of finite slope. This is expected from the nonparabolicity mechanism for nondegenerate material at high magnetic fields [Eq. (14)] or degenerate material with low concentration [Eq. (27)]. As can be seen from Table I, the sample having $N=6\times10^{14}$ cm^{-3} is nondegenerate while the two higher concentration samples are slightly degenerate at liquid-nitrogen temperatures. At these magnetic fields (above 50 kG) the degenerate samples easily satisfy the criterion Eq. (25) of low concentration used to derive Eq. (27). If, on the other hand, this transition were primarily due to the inversion-asymmetry mechanism, then the integrated absorption for the nondegenerate sample should be independent of magnetic field [Eq. (22)] and for the degenerate samples should depend *inversely* on H^2 [Eq. (31)].

In Fig. 6, $\alpha\Delta H/N$ is plotted versus H^2 at liquid-nitrogen and liquid-helium temperatures for a sample having 6×10^{15} electrons/cm^3. Except for a slight shift to higher values at helium temperature, the data are almost identical. The difference is probably due to effects of the localized electrons which are still strong for these magnetic fields at liquid-helium temperatures. The helium-temperature data also show an anomaly between 60 and 65 kG although it appears relatively weaker in these data. The anomaly was also observed in the other samples at liquid-helium temperatures.

The integrated absorption obtained for four samples having electron concentrations at liquid-nitrogen temperature between 1.5×10^{14} and 1.5×10^{16} cm^{-3} is plotted as a dimensionless parameter $\alpha\Delta H/(\nu_{c,s}/c)H$ versus N in Fig. 7 on a log-log scale. Each point is an average of three values at different magnetic fields. The solid straight line is a line of unity slope drawn through the experimental points. Thus over these two decades in concentration, the integrated absorption depends linearly on concentration. This behavior is expected for the nonparabolicity mechanism for both degenerate and nondegenerate samples, but for the inversion-asymmetry mechanism only nondegenerate samples are expected to have this concentration dependence, the intensity of degenerate samples being proportional to N^3 [Eq. (31)]. Since the two lower concentration samples are nondegenerate, and the two higher concentration samples degenerate at liquid-nitrogen temperature, Fig. 7 is consistent only with the nonparabolicity mechanism.

It is apparent from the preceding that the primary mechanism allowing combined resonance in InSb is that of nonparabolicity. A quantitative comparison of the calculated and observed integrated absorption is of interest. For a sample having 6×10^{14} electrons/cm^3 at liquid-nitrogen temperatures, Eq. (14) yields a value of 29 cm^{-1} kG for $(\alpha_3\Delta H)_{NP}$ in a magnetic field of 90 kG using the values of Pidgeon *et al.*[24] for the band parameters. The measured value is 10 cm^{-1} kG, in reasonable agreement.

We now turn our attention to the anomaly observed in the plots of integrated intensity versus H^2. This was observed in all samples studied at both liquid-nitrogen and liquid-helium temperatures, and seems to be a real effect, not the result of any systematic experimental error. The anomaly appears as both an increase in peak absorption constant and a simultaneous broadening of the line. This behavior is similar to that observed in

[24] C. R. Pidgeon, D. L. Mitchell, and R. N. Brown, Phys. Rev. **154**, 737 (1967).

cyclotron and combined resonance at lower fields[25–28] and attributed to coupling with one LO phonon. However, in these experiments a splitting of the line into two or more modes is observed simultaneously with the broadening immediately above the coupling energy. No such splitting of the absorption line was observable in the present data. At the magnetic fields where the anomaly occurs, the energy separation of the levels are such that there are several possible *multiphonon* processes that might account for the effect. Two zone-center LO phonons (energy 392 cm^{-1}) could couple the final state ($L=1$, spin down) to the initial state ($L=0$, spin up) with energy separation ~ 400 cm^{-1} at 60 kG. A zone-center LO phonon and two W point TA phonons (energy 293 cm^{-1}) could couple the final state ($L=1$, spin down) to the $L=0$, spin-down state (energy separation 290 cm^{-1} at 60 kG). Finally, two TA phonons at point W (energy 83 cm^{-1}) could couple the final state ($L=1$, spin down) to the $L=1$, spin-up state (energy separation 81.5 cm^{-1} at 60 kG). There are no one-phonon processes energetically possible in this region. The multiple-phonon processes described above are all expected to be quite weak, the first and last because they involve a spin flip and the second because it is a three-phonon process. Unfortunately, the data are not sufficiently good to allow more than this rather sketchy outline of possible mechanisms.

In the process of studying an anisotropy in the position of the combined resonance line[29] in a sample with $N=8\times10^{14}$ electrons/cm^3, an anisotropy in the integrated absorption was also observed. At 90 kG and liquid-nitrogen temperatures, when the applied magnetic field was rotated from the [100] to the [111] crystalline axes, the peak absorption increased by approximately 20%. When the temperature was lowered to 8–10°K, this anisotropy increased to 35%. There was no appreciable change in the percentage anisotropy when the magnetic field was lowered to slightly less than 70 kG. The liquid-nitrogen temperature line also appeared to broaden slightly going from $\mathbf{H}\|[100]$ to $\mathbf{H}\|[111]$. The liquid-helium-temperature data are complicated by the existence of both impurity-shifted and free-carrier combined resonance lines, thus making linewidth measurements impractical.

The origin of this anisotropy is not well understood since the nonparabolicity mechanism is isotropic except for the small ($\sim 1.7\%$ at 90 kG) anisotropy in the field position of the combined resonance line at constant energy. The possibility that this is a result of contributions from the anisotropic inversion-asymmetry mechanism (it has the appropriate angular dependence) may be discounted for several reasons. First, calculations of the relative magnitudes assuming $\delta_0 \sim 200$ a.u. indicate the contribution of the inversion asymmetry to be at most 2% of the nonparabolicity intensity. This is, in fact, an overestimate of δ_0 as is indicated by unsuccessful attempts to observe the inversion-asymmetry-allowed transition at photon energy $h\nu = h(2\nu_c + \nu_s)$. Second, reducing the magnetic field from 90 to as little as 35 kG had only a very slight effect on the anisotropy. If it were due to inversion asymmetry, the anisotropy should have increased by a factor of about 6. Finally, a reduction from liquid-nitrogen to liquid-helium temperature should decrease the relative importance of the inversion-asymmetry mechanism, whereas a relative *increase* is observed. Since the intensity anisotropy cannot be due to the effects mentiond above and possible experimental effects have been ruled out, it seems that only by resorting to higher-order terms in the effective Hamiltonian can this anisotropy be explained.

We now turn our attention to the spin-flip transition of energy $h\nu_s(0)$. A search for this transition was made in the vicinity of 50 kG in several samples with electron concentrations between 10^{14} and 10^{16} cm^{-3}. Most of these experiments were performed at liquid-helium temperatures where the materials are degenerate before it was realized that a significant increase in intensity is expected for nondegenerate material. For a nondegenerate system we see from Fig. 3 that the integrated absorption for this transition is only a factor of 7 weaker than the integrated absorption at energy $h\nu_{c,s}$, whereas for degenerate material the intensity is weaker by a factor of 1500 under the conditions discussed in Sec. II B 2(*a*). No transition was observed at liquid-helium temperature. At a temperature of ~ 80°K, however, a very weak transition was observed at several magnetic fields in the vicinity of 50 kG in a sample 4-mm thick having a carrier concentration of about 6×10^{14} cm^{-3}. The energy of this transition agrees within experimental error with values for $h\nu_s(0)$ obtained as discussed in the next section. A rough estimate of the integrated intensity yields a value of 0.6 cm^{-1} kG. This is to be compared with a calculated value of 1.3 cm^{-1} kG, which is in quite reasonable agreement. Since the data are rather marginal, no further discussion will be presented at this time.

A number of unsuccessful attempts were made to find the other transitions predicted by the inversion-asymmetry mechanism. It is not too surprising that the inversion-asymmetry-allowed transitions were not observed since they are expected to be much weaker than the nonparabolicity-allowed transitions. A careful search was made at liquid-helium temperature in an unoriented sample 1.5-mm thick having 6×10^{15} electrons/cm^3 with $\mathbf{E}\|\mathbf{H}$ and $\mathbf{E}\perp\mathbf{H}$. There was no evidence of the transitions at photon energy

[25] D. H. Dickey, E. J. Johnson, and D. M. Larsen, Phys. Rev. Letters **18**, 599 (1967).
[26] C. J. Summers, P. G. Harper, and S. D. Smith, Solid State Commun. **5**, 615 (1967).
[27] D. H. Dickey and D. M. Larsen, Phys. Rev. Letters **20**, 65 (1968).
[28] B. D. McCombe and R. Kaplan, Phys. Rev. Letters **21**, 756 (1968).
[29] B. D. McCombe, Solid State Commun. **6**, 533 (1968).

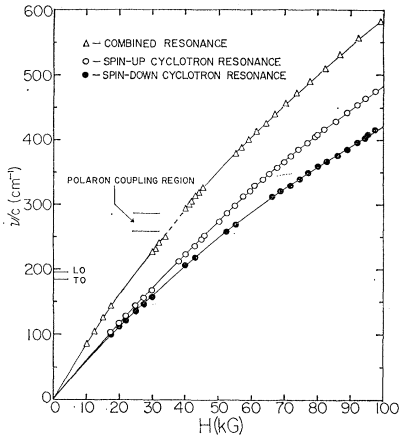

FIG. 8. Experimentally measured photon energy (in wave numbers) versus magnetic field for combined resonance ($h\nu_{c,s}$), spin-up cyclotron resonance [$h\nu_c(\uparrow)$], and spin-down cyclotron resonance [$h\nu_c(\downarrow)$]. Energies are as defined in Fig. 2. The region where polaron coupling causes a splitting into two branches in the combined resonance data is indicated. Data cannot be obtained in a band around the reststrahlen region indicated by LO and TO in the figure.

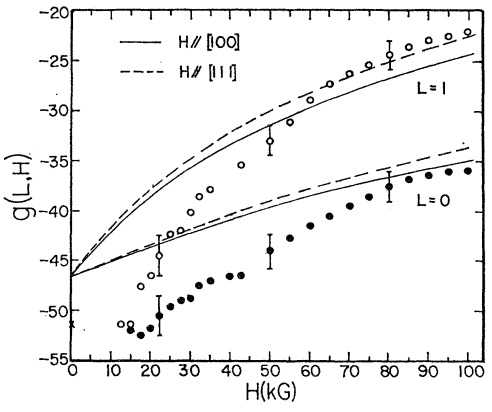

FIG. 9. Experimental g values versus magnetic field for the lowest two Landau levels in InSb. The procedure for obtaining the g values from the data is described in the text. Error bars are shown at three representative values of magnetic field. The solid and dashed lines are the results of the calculation of Pidgeon *et al.* (Ref. 24).

$h\nu=h(2\nu_c+\nu_s)$ even though weak transitions at energies $h(2\nu_c)$, $h(\nu_c+\nu_{LO})$, and $h(2\nu_c+\nu_{LO})$ were readily observed in the $\mathbf{E}\perp\mathbf{H}$ polarization. From this negative result an upper limit may be set on the parameter δ_0. This will be discussed in the next section. After the measurements were completed, Fan and Saleh[30] observed a weak transition of approximate energy $h(2\nu_c+\nu_s)$ in a sample having a carrier concentration of slightly less than 10^{16} cm^{-3}. This observation is not inconsistent with the present data since alignment close to the maximum in the angular function of intensity and a higher-mobility sample could account for an increase of as much as a factor of 20 in the peak-absorption constant.

B. Band-Structure Results

In addition to testing the theoretical models, studies of the combined resonance transition at energy $h\nu_{c,s}$ in conjunction with other intraband transitions provide a direct measurement of the conduction-band g values in InSb. As is shown in Fig. 2, the difference between the combined resonance and spin-up cyclotron resonance energies, $h\nu_{c,s}-h\nu_c(\uparrow)$, yields the spin energy of the $L=1$ Landau level, $h\nu_s(1)$; similarly, the difference between the combined resonance and spin-down cyclotron resonance energies, $h\nu_{c,s}-h\nu_c(\downarrow)$, gives the spin energy of the $L=0$ Landau Level, $h\nu_s(0)$. Combined resonance and spin-up and spin-down cyclotron resonance were observed at magnetic fields between 15 and 100 kG. The results are shown in Fig. 8, where the free-electron transition energies in cm^{-1} are plotted versus magnetic field. Smooth curves are drawn through each set of points. Experimental points were obtained for $\mathbf{H}\|[111]$, and most of the data were obtained near liquid-nitrogen temperature. From the smooth curves in Fig. 8, one obtains the energy difference $h\nu_s(0)$ and $h\nu_s(1)$ at constant magnetic field, and the g values are calculated from the expression

$$h\nu_s(L,H)=g(L,H)\beta H,$$

where β is the Bohr magneton. Results of the calculations are shown in Fig. 9, where the free-carrier electron g values are plotted increasing negatively downward versus magnetic field. Representative error bars are included at several values of magnetic field. The solid and dashed lines are the results of Pidgeon *et al.*'s[24] computer fit to interband data for the indicated orientations. At high magnetic fields the experimental points are in reasonable agreement with the calculations. However, below about 50 kG there is a significant deviation of the experimental results from calculated curves, the experimental points being larger in absolute value. Patel and Slusher[31] have also obtained similar results for the $L=0$ g value from Raman-scattering experiments. The present measurements at low fields are in reasonable agreement with recent microwave ESR measurements[32] (indicated by the symbol X in Fig. 9) and also with earlier work.[11,12] The reason for this discrepancy is not well understood, but it may mean that corrections due to higher bands become less important at low fields, i.e., the calculations have weighted the higher-band interactions too heavily at low fields.

The detailed calculations of Pidgeon *et al.*[24] indicate an anisotropy in the conduction-band g values as is shown by the solid and dashed lines in Fig. 9. A perturbation calculation by Ogg[18] yields similar results. In the latter treatment the anisotropy arises from the

[30] H. Y. Fan and A. S. Saleh (private communication).

[31] C. K. N. Patel and R. E. Slusher (private communication).

[32] R. A. Isaacson, Phys. Rev. **169**, 312 (1968).

last term of Eq. (1) and is the result of higher-band interactions. The maximum anisotropy is predicted to occur when the applied magnetic field is totated from the [100] to the [111] crystalline axes with the smallest (in magnitude) g value for $\mathbf{H}\|[111]$. Experimental measurements[29] of the anisotropy of the position of the combined resonance transition of energy $h\nu_{c,s}$ at several values of magnetic field have given the anisotropies of the $L=0$ and $L=1$ g values. These results are in good agreement with the calculations.

One final bit of information concerning the band structure of InSb may be inferred from the negative result in the search for the transition of energy $h(2\nu_c+\nu_s)$. The integrated absorption for this transition may be calculated in the manner of Sec. II. The result for a degenerate electron gas with low concentration is given by

$$(\alpha_3\Delta H)_{IA}=\frac{100\pi^2e^2\delta_0^2\eta^2|B_{(333)}|^2}{9\hbar^5cn}NH \qquad (35)$$

for $\mathbf{E}\|\mathbf{H}$. The angular function $|B_{(333)}|^2$ has zeros in the [100] and [111] directions and maxima in the [110] directions with a maximum value of 9/8.[3] The other polarizations have comparable maximum values of angular functions. The sensitivity of the measurements was such that a transition with an integrated absorption of $\alpha\Delta H\geq 0.25$ cm^{-1}—kG would have been observable for a linewidth of about 4 kG. Taking a value of $|B_{(333)}|^2$ of 0.1 as a lowest probable limit for the unoriented sample studied (H was perpendicular to [111] but not parallel to any principal axis) and substituting values into Eq. (35) we obtain 50 a.u. as a conservative upper limit to δ_0. This is in fair agreement with a value of 70 obtained from recent studies[33] of ESR linewidths as a function of concentration in InSb at 2-mm wavelength.

[33] M. S. Folgeson (private communication).

V. CONCLUSIONS

The present experiments have demonstrated conclusively that the primary mechanism allowing combined resonance transitions in InSb is nonparabolicity. In addition, studies of combined resonance have allowed a determination of details of the band structure of InSb; in particular the g values of the lowest two Landau levels were measured over a wide range of magnetic fields. Since nonparabolicity is the dominant mechanism, combined resonance should be observable in semiconductors having a large spin-orbit interaction, a small fundamental energy gap, and a center of inversion symmetry. The most likely candidate from this point of view is PbTe. However, there are several circumstances, most notably the coincidence of infrared frequencies of interest and the reststrahlen region, which make actual experimentation very difficult. Of course other III-V semiconductors are also possibilities. Preliminary experiments in a sample of InAs with rather poor mobility have revealed broad absorption peaks having the correct polarization properties ($\mathbf{E}\|\mathbf{H}$) and approximately the expected energy of the combined resonance transition. Further experiments are in progress to verify this.

ACKNOWLEDGMENTS

The author would like to express his appreciation to S. G. Bishop and R. Kaplan for assistance in many aspects of this work. Thanks are also due S. Teitler, D. L. Mitchell, and R. F. Wallis for helpful discussions.